Appl. Phys. A (2016) 122:349
DOI 10.1007/s00339-016-9906-0

Applied Physics A
Materials Science & Processing

Temperature dependence of band gap ratio and Q-factor defect mode in a semiconductor quaternary alloy hexagonal photonic-crystal hole slab

R. Sánchez-Cano[1] · N. Porras-Montenegro[2]

Received: 20 August 2015 / Accepted: 26 November 2015 / Published online: 10 March 2016

Abstract We present numerical predictions for the photonic TE-like band gap ratio and the quality factors of symmetric localized defect as a function of the thickness slab and temperature by the use of plane wave expansion and the finite-difference time-domain methods. The photonic-crystal hole slab is composed of a 2D hexagonal array with identical air holes and a circular cross section, embedded in a non-dispersive III–V semiconductor quaternary alloy slab, which has a high value of dielectric function in the near-infrared region, and the symmetric defect is formed by increasing the radius of a single hole in the 2D hexagonal lattice. We show that the band gap ratio depends linearly on the temperature in the range 150–400 K. Our results show a strong temperature dependence of the quality factor Q, the maximum ($Q = 7000$) is reached at $T = 350$ K, but if the temperature continues to increase, the efficiency drops sharply. Furthermore, we present numerical predictions for the electromagnetic field distribution at $T = 350$ K.

1 Introduction

Optoelectronics devices operating in the infrared range arouse a growing interest due to their potential applications in optical telecommunications, atmospheric pollution monitoring, industrial process control, medical diagnoses, optomechanical systems, characterization of materials, analysis of biological samples, biomedical applications, and chip light manipulation [1–6]. Recently, much interest has been drawn in semiconductor photonic-crystal hole slabs in which the structure is formed by a 2D hexagonal lattice. The advantage of a semiconductor photonic-crystal hole slab is that in addition to providing light guided modes and photonic gaps for some frequency ranges for the TE-like or TM-like polarization modes, it also allows the easy inclusion of defects and efficient light emitters into the crystal [7, 8]. In semiconductor-based photonic-crystal hole slabs can make important contributions to the design of new devices operating in the near-infrared range [9–14]. Several theoretical studies have been carried out on binary semiconductor photonic-crystal slabs. However, few theoretical results on III–V quaternary semiconductor photonic-crystal slabs have been reported. In this theoretical work using supercell plane wave expansion (SCPW) and the finite-difference time-domain (FDTD) methods [15–20], we have calculated the photonic band gap ratio and Q-factor as a function of temperature, and the electromagnetic field distribution for electromagnetic waves propagating in a semiconductor photonic-crystal hole slab composed of a 2D hexagonal array with identical air holes and a circular cross section, and a symmetric point defect, embedded in a non-dispersive $Ga_{1-x}In_xAs_ySb_{1-y}$ semiconductor quaternary alloy slab.

The paper is organized as follows: In Sect. 2.1, we briefly describe the mathematical setting of band structure calculation by the use of a supercell plane wave expansion method. In Sects. 2.2 and 2.3, we present the FDTD basis to calculate spatial distribution of the electromagnetic fields. Numerical parameter, results and discussion are presented in Sect. 3. Finally, we conclude in Sect. 4.

✉ R. Sánchez-Cano
rsanchez40@gmail.com

[1] Departamento de Física, Universidad Autónoma de Occidente, 2790 Cali, Colombia

[2] Departamento de Física, Universidad del Valle, 25360 Cali, Colombia

2 Theoretical framework

2.1 Supercell plane wave method

Using the Bloch theorem and Fourier series expansion for electromagnetic fields and dielectric function, $\varepsilon(\vec{r}, \mathrm{x}, T)$ in a 3D periodic medium and Maxwell's equations, after some algebra, we obtain the following equations for the expansions coefficients $\vec{E}_K(\vec{G})$ and $\vec{H}_K(\vec{G})$:

$$-\sum_{\vec{G}'} k(\vec{G}-\vec{G}')(\vec{K}+\vec{G})\times[(\vec{K}+\vec{G}')\times\vec{E}_{\vec{K}}(\vec{G}')] = \frac{\omega^2_{\vec{K},m}}{c^2}\vec{E}_{\vec{K},m}(\vec{G}), \tag{1}$$

$$-\sum_{\vec{G}'} k(\vec{G}-\vec{G}')(\vec{K}+\vec{G})\times[(\vec{K}+\vec{G}')\times\vec{H}_{\vec{K}}(\vec{G}')] = \frac{\omega^2_{\vec{K},m}}{c^2}\vec{H}_{\vec{K},m}(\vec{G}), \tag{2}$$

with,

$$k(\vec{G}) = \frac{1}{V_0}\int_{V_0} d\vec{r}\,\frac{1}{\varepsilon(\vec{r}, \mathrm{x}, T)}\exp(i\vec{G}\cdot\vec{r}), \tag{3}$$

where V_0 denotes the volume of the unit cell of the photonic crystal, $\vec{r}$ is the position vector, x is the Indium concentration, T is the absolute temperature, $\vec{K}$ and $\vec{G}$ are the reciprocal lattice vectors, ω and c are the frequency of the electromagnetic wave and the speed of light, respectively.

As suggested by Samara [21] it is not likely that the quantity $\varepsilon(\vec{r}, x, T)$ is really linearly dependent on temperature over a broad temperature range. Therefore, we fit the dependence of such quantity by Varshni-type equation given by

$$\varepsilon(\vec{r}, \mathrm{x}_i, T) = \varepsilon(\vec{r}, \mathrm{x}_i, 0) + \frac{\delta T^2}{\eta + T}, \quad 0 \le \mathrm{x}_i \le 1, \tag{4}$$

with $\delta = 4.8\times10^{-3}\,\mathrm{K}^{-1}$, $\eta = 550\,\mathrm{K}$ [22]. The parameter $\varepsilon(\vec{r}, \mathrm{x}_i, 0)$ for a given concentration $x = x_i$ is determined by evaluating equation (4) at $T = 300\,\mathrm{K}$ and the expression proposed by Mikhailova [23]. Thus, we can obtain the static dielectric constant value of the quaternary alloy for concentration, $x = x_i$. We propose the dielectric constant as a function of the temperature T, at $x = 0.16$ for the quaternary alloy, as [24]

$$\varepsilon(\vec{r}, 0.16, T) = 13.6 + \frac{4.8\times10^{-3}T^2}{550+T}. \tag{5}$$

From Eqs. (1), (2), and (5) we can obtain the photonic band structure solving the eigenvalue equations numerically for each value of $\vec{K}$ and for each value of the band index m. The kernel of the supercell method of expansion in plane waves is constructed considering the periodic arrangement of the photonic-crystal slab along the y-direction with a period aN, while in the $x-z$ plane the structure is a 2D periodic lattice with period, a, with a symmetric point defect. Supercell method in the $x-z$ plane also is used to calculate defective modes [15].

The K_y component of a wave vector $\vec{K}$ is restricted to the interval $(-\pi/aN) < K_y < (-\pi/aN)$ in a first 3D Brillouin zone and tends to zero when the supercell size aN increases; then, the wave vector is chosen in the form $\vec{K} = (K_x, 0, K_z)$. As long as the domain in the y-direction is sufficiently large, the coupling between the modes of the adjacent slabs is negligible, and the eigenmodes converge to the correct results for just one plane of holes. In general, the modes of a 3D-photonic crystal are hybrid and involve six components $(E_x, E_y, E_z, H_x, H_y, H_z)$. However, the separation of Maxwell's equations into E-polarization (TM: transversal magnetic mode) and H-polarization (TE: transversal electric mode) is only possible for 1D and 2D photonic crystals. The 3D periodic hole slab possesses $\hat{\sigma}_x, \hat{\sigma}_y$ and $\hat{\sigma}_z$ reflection symmetries; then, an analogous classification of the modes is possible with respect to reflection in the $y = 0$ plane. Therefore, even $(\vec{E} = (E_x, 0, E_z);\ \vec{H} = (0, H_y, 0))$ and odd $(\vec{E} = (0, E_y, 0);\ \vec{H} = (H_x, 0, H_z))$ modes at $y = 0$ are the analog of TE and TM modes, respectively. Figure 1 shows the profile of the hole slab (left) and k-path in the first Brillouin zone of the 2D hexagonal lattice at $K_y = 0$ plane (right), and the system is invariant under reflections through the $y = 0$ plane, which allows us to classify the modes in even (TE-like) and odd (TM-like).

2.2 FDTD method

A 3D-FDTD method is used to calculate field distribution, the frequency, power spectrum transmittance, and coupled modes.

The unit cell configuration for the FDTD calculation and elementary lattice vectors $\vec{a}, \vec{b}$ are shown in Fig. 2.

We consider a plane wave packet of Gaussian time dependence uniform in the y-direction passing through the hexagonal array in $x-z$ plane. The wave packet is a set of plane waves with different frequencies, named Gaussian modulated continuous wave (GMCW), where the incident field for each input point has the form

$$F_y^{\mathrm{inc}}(x, z_{\mathrm{inc}}) = AF(x, z_{\mathrm{inc}})\exp\left[-\left(\frac{t-t_0}{2W}\right)^2\right]\sin(\varpi t), \tag{6}$$

where A is the field amplitude, $F(x, z_{\mathrm{inc}})$ is the rectangular transverse field spatial distribution at the incident plane location z_{inc}, t is the time, t_0 is the time offset, W is the

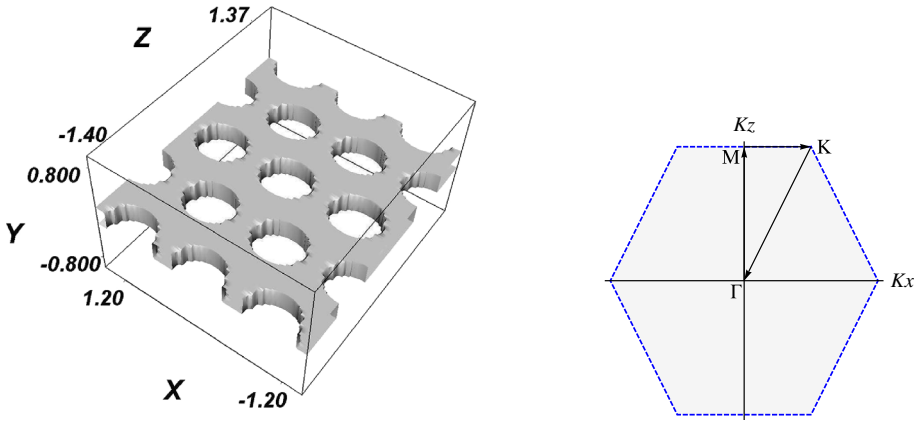

Fig. 1 (Color online) *Left* Schematic illustration of the photonic-crystal hole slab composed of a 2D hexagonal array with identical air holes and a circular cross section, fabricated in a $Ga_{0.84}In_{0.16}As_{0.14}Sb_{0.86}$ semiconductor quaternary alloy slab. *Right* k-path in the first Brillouin zone of the 2D hexagonal lattice at $K_y = 0$ plane; Γ, M, and K are the three high-symmetry points

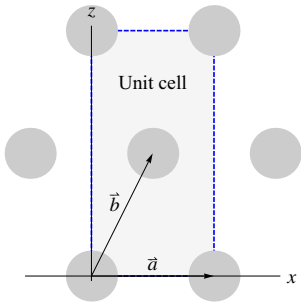

Fig. 2 (Color online) 2D schematic illustration of the photonic-crystal hole slab composed of a hexagonal array with identical air holes and a circular cross section, fabricated in a $Ga_{0.84}In_{0.16}As_{0.14}Sb_{0.86}$ semiconductor quaternary alloy slab; the *shaded rectangle* shows the FDTD unit cell at $K_y = 0$ plane

pulse half width parameter, and $\varpi = 2\pi c/\lambda$ is the carrier frequency of the input wave.

For the numerical band structure and the field distribution calculations Bloch periodicity in $\pm x$, y, z-directions are the boundary conditions used in this work. Perfect Matched Layer (PML) in $\pm z$-direction are the boundary conditions used for the transmittance spectra calculation [16, 19, 20].

2.3 Power transmittance and quality factor

For an electromagnetic wave propagating in the $x-z$ plane, the power can be obtained by the flux of the Poynting vector through any $x-y$ plane near the FDTD absorbing boundaries (PML). The total power through the $x-y$ plane at the z position can be calculated for TE and TM modes as

$$P_{\mathrm{TE}} = \mathrm{Re}\left(\frac{1}{2}\int_s (\check{E}_x + \check{E}_z) \times H_y^* \mathrm{d}x\mathrm{d}y\right), \tag{7a}$$

$$P_{\mathrm{TM}} = \mathrm{Re}\left(\frac{1}{2}\int_s \check{E}_y \times (H_x^* + H_z^*)\mathrm{d}x\mathrm{d}y\right), \tag{7b}$$

where $\check{E}$ is the complex value that comes from the discrete Fourier transform (DFT) calculation and H^* is the complex conjugate value. We calculate the power normalized to the input signal given by Eq.(6).

The quality factor Q of the point defect is defined as

$$Q = \omega_0 \frac{U}{P_{\mathrm{abs}}}, \tag{8}$$

where U is the stored energy in the resonant mode with frequency ω_0 and P_{abs} is the power absorbed in the boundaries.

3 Results and discussion

For numerical calculations, the following parameters were considered: The PWM convergence tolerance for the eigenvalues of the Eqs. (1) and (2)was 10^{-12}. Therefore, the precision obtained in the frequency was roughly the square root of the convergence tolerance, the carrier wavelength of the input wave $\lambda = 1.5\,\mu\mathrm{m}$, lattice constant $a = 1\,\mu\mathrm{m}$, hole radius $r = 0.45a\,\mu\mathrm{m}$, dielectric function of the background material $\varepsilon = 1$ (air), dielectric function of the $Ga_{0.84}In_{0.16}As_{0.14}Sb_{0.86}$ semiconductor slab $\varepsilon(\vec{r}, 0.16, 300) = 14.1$ is given by Eq.(5).

The excited Gaussian pulse was given by Eq. (6), with $A = 1, F(x, z_{\mathrm{inc}}) = 0$ if $|x - x_{\mathrm{inc}}| > 6\,\mu\mathrm{m}$ else $F(x, z_{\mathrm{inc}}) = 1, t_0 = 9.94 \times 10^{-15} s, W = 2.81 \times 10^{-15} s$, and $\varpi = 1.26 \times 10^{15}\,\mathrm{rad/s}$ in the $\Gamma - M$ direction. For the power transmittance, the computational domain $\pm z$ was truncated by ten additional PML layers with 1×10^{-12} theoretical reflection coefficient. The space cell size was taken as $\Delta x = \Delta z = 0.008\,\mu\mathrm{m}$ and the time step size was selected as $\Delta t = 1.779 \times 10^{-17}\,\mathrm{s}$ that satisfies the FDTD stability limit [19, 20]. Figure 3a shows the photonic band structure for the lowest even modes and Fig. 3b shows the photonic band structure for the lowest odd modes, both even and odd modes calculated by the PWM method for periodic slab. The photonic bands are presented along the $\Gamma - \mathrm{M} - \mathrm{K} - \Gamma$ edge of an irreducible Brillouin zone

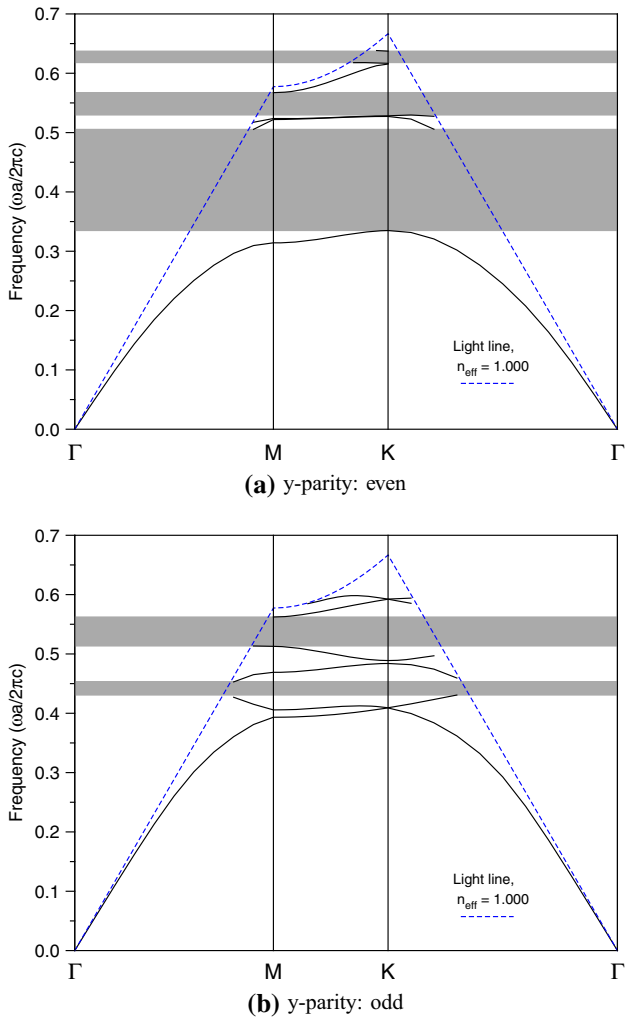

Fig. 3 (Color online) Photonic band structure of a $Ga_{0.84}In_{0.16}As_{0.14}Sb_{0.86}$ periodic hexagonal photonic-crystal hole slab; **a** even modes and **b** odd modes. The slab dielectric constant is 14.1, its thickness is $d = 0.6a$, the air rods radius is $r = 0.45a$, and the cladding background is air

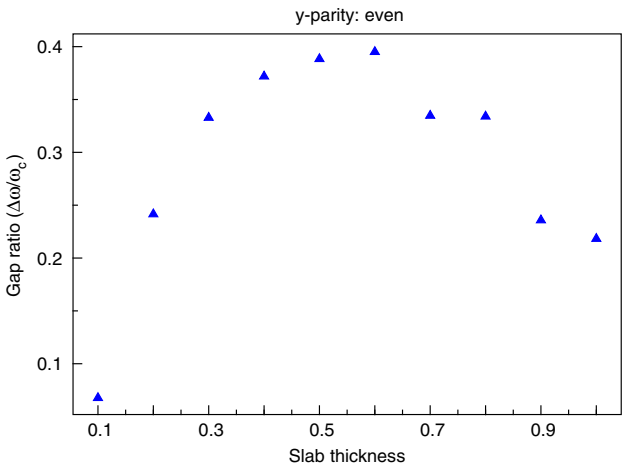

Fig. 4 (Color online) Band gap ratio, $\triangle\omega/\omega_c$ for TE-like modes as a function of the slab thickness d, for $Ga_{0.84}In_{0.16}As_{0.14}Sb_{0.86}$ slab, ω_c is the frequency at the center of the gap. The slab dielectric constant is $\varepsilon(\vec{r}, 0.16, 300) = 14.1$, the air rods radius is $r = 0.45a$, and the cladding background is air

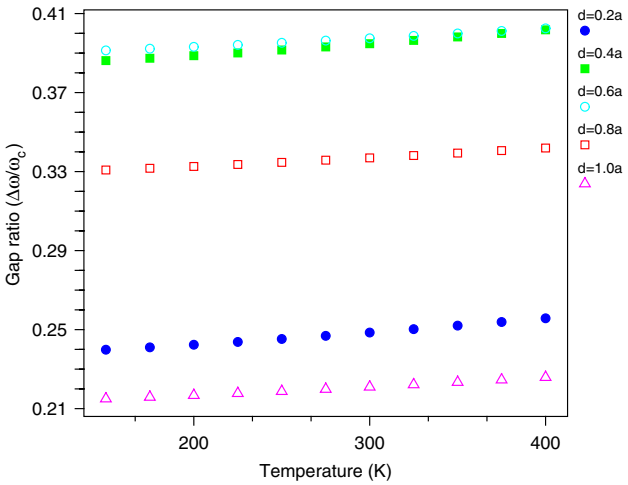

Fig. 5 (Color online) Band gap ratio, $\triangle\omega/\omega_c$ for TE-like (even) modes as a function of the temperature for slab thickness $d = 0.2a, d = 0.4a, d = 0.6a, d = 0.8a$, and $d = 1.0a$, and the same parameters as in Fig. 4

(Right in Fig. 1). As it is seen, the $Ga_{0.84}In_{0.16}As_{0.14}Sb_{0.86}$ periodic hexagonal photonic-crystal hole slab has a wide band gap (gray zone) in the even modes (electric field in the x–z plane). This characteristic is observed at $\omega a/2\pi = 0.33 - 0.51$. Nevertheless, this is not an authentic band gap because radiation modes exist above the light line (dashed line) in the same frequency range. Conversely, Fig. 3b shows a small band gap in the odd modes (magnetic field in the x–z plane). This feature is observed in a hole hexagonal photonic-crystal slab because even and odd modes have close similarities in TE and TM modes of the 2D hexagonal photonic crystal, respectively.

Figure 4 shows a graph of the band gap ratio, $\triangle\omega/\omega_c$ for even modes as a function of slab thickness d at room temperature for the $Ga_{1-x}In_xAs_ySb_{1-y}$, ω_c is the frequency at the center of the gap. As observed, there is an optimal thickness at $d = 0.6a$, which justifies the use of slab thickness $d = 0.6a$ in our calculations for $r = 0.45a$. The existence of an optimum thickness can be understood by considering two limiting cases of a very thin or very thick slab. If the slab is too thin, practically there are no guided modes and the lattice periodicity do not affect the cladding. On the other hand, if the slab is very thick, the photonic band gap approaches to the 2D photonic-crystal case. However, higher modes are pulled into the photonic band gap.

Figure 5 shows a graph of the band gap ratio, $\triangle\omega/\omega_c$ for even modes as a function of the temperature for slab thickness, $d = 0.2a, d = 0.4a, d = 0.6a$, $d = 0.8a$, and $d = 1.0a$, radius $r = 0.45a$, Indium and Arsenic

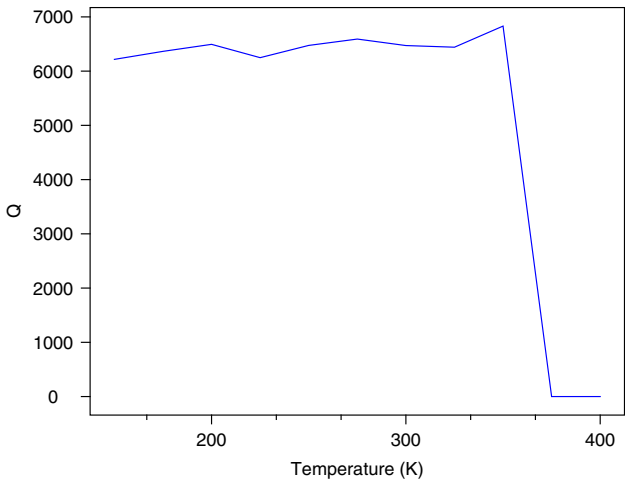

Fig. 6 (Color online) Q-factor for TE-like mode as a function of the temperature for $\omega_0 a/2\pi C = 0.24$, slab thickness $d = 0.6a$, defect radius $r_d = 0.45a$ and lattice radius $r = 0.3a$

concentrations, $x = 0.16$ and $y = 0.14$, respectively. We see that in the graphs the band gap ratio depends linearly on the temperature. This result is due basically to the dielectric constant, which is strongly linked to the electronic energy band structure of the semiconductor quaternary alloy and to the variation in the critical point energy levels, originated by the lattice thermal expansion and Debye–Waller effect. Furthermore, an analysis shows that the dielectric constant increases linearly with the temperature in 150–400 K range.

Figure 6 shows a strong temperature dependence of the quality factor Q; the maximum ($Q = 7000$) is reached at $T = 350$ K, but if the temperature continues to increase the efficiency drops sharply. At $T = 350$ K the dielectric function is no longer linear, and the quality factor begins to decrease, because the vertical radiation losses in the cavity become large. To have a better understanding of the results previously obtained, in Fig. 7. we show the distribution of electric field intensity in the center of the slab, $y = 0$, and in the upper border, $y = d/2$. As shown, the energy into the cavity ($y = 0$) at $\omega_0 a/2\pi C = 0.24$ is smaller than the energy radiated vertically ($y = d/2$). This result agrees with other reported for InSb [15, 25].

4 Conclusions

We show that the band gap ratio depends linearly on the temperature in the range 150–400 K. As observed, higher values are obtained for a thickness $d = 0.6a$. Furthermore, we show that there is a strong temperature dependence of the quality factor Q, and the maximum value of the quality factor Q ($Q = 7000$) is reached at $T = 350$ K, but if the temperature continues to increase, the efficiency drops sharply. In conclusion, our theoretical predictions allow a better understanding of this type of photonic crystals based on quaternary semiconductors $Ga_{1-x}In_xAs_ySb_{1-y}$ periodic hexagonal photonic-crystal hole slab and their applications for the design of new temperature-tunable optoelectronic devices in the infrared spectrum.

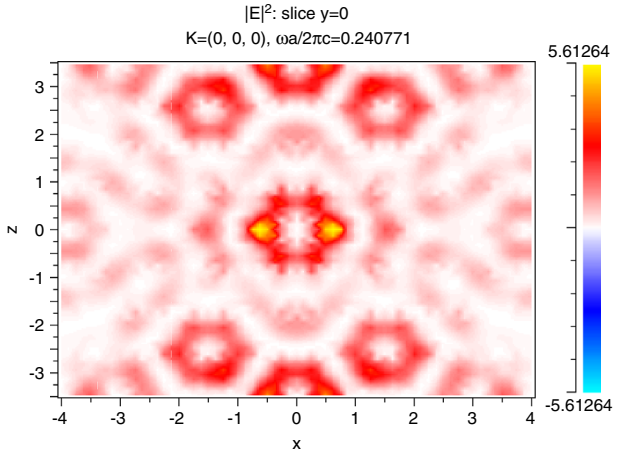

(a) y-parity: even, y = 0

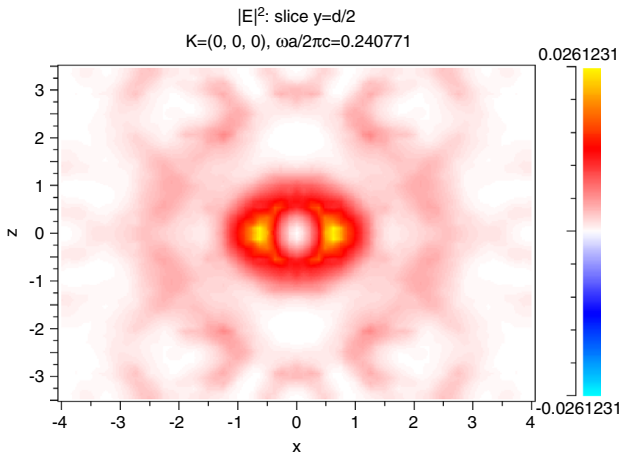

(b) y-parity: even, y = d/2

Fig. 7 (Color online) Distribution of electric field intensity at $T = 350$ K in the center of the slab, $y = 0$ (**a**), and in the upper border, $y = d/2$ (**b**) of a $Ga_{0.84}In_{0.16}As_{0.14}Sb_{0.86}$ defect mode hexagonal photonic-crystal hole slab. The slab dielectric constant is 14.1, its thickness is $d = 0.6a$, the air rods radius is $r = 0.45a$, and the cladding background is air

Acknowledgments The authors thank Dirección de Investigaciones y Desarrollo Tecnológico Universidad Autónoma de Occidente and Vicerrectoría de Investigaciones Universidad del Valle for partial financial support under the Grant Numbers 10INTER-132 and CI:7871, respectively.

References

1. A. Joullié, P. Christol, A.N. Baranov, A. Vicet, Solid-state mid-infrared laser sources, in I.T. Sorokina, K.L. Vodopyanov, (eds.), *Topics in Applied Physics*, vol. 89 (Springer, Germany, 2003), pp. 1–59

2. G. Ru, Y. Zheng, A. Li, The wavelength shift in GaInAsSb photodiode structures. J. Appl. Phys. **77**, 6721 (1995)
3. O. Levi, W. Suh, M.M. Lee, J. Zhang, S.R.J. Brueck, S. Fan, J.S. Harris, Integrated biomedical nanosensor using guided resonance in photonic crystal structures. Proc. Spie **6095**, 60950N (2006)
4. C.H. Bui, J. Zheng, S.W. Hoch, L.Y.T. Lee, J.G.E. Harris, C.W. Wong, High-reflectivity, high-Q micromechanical membranes via guided resonances for enhanced optomechanical coupling. Appl. Phys. Lett. **100**, 021110 (2012)
5. Y. Nazirizadeh, J. Reverey, U. Geyer, U. Lemmer, C. Selhuber-Unkel, M. Gerken, Material-based three-dimensional imaging with nanostructured surfaces. Appl. Phys. Lett. **102**, 011116 (2013)
6. E. De Tommasi, A.C. De Luca, S. Cabrini, I. Rendina, S. Romano, V. Mocella, Plasmon-like surface states in negative refractive index photonic crystals. Appl. Phys. Lett. **102**, 081113 (2013)
7. H. Kurt, E. Colak, O. Cakmak, H. Caglayan, E. Ozbay, The focusing effect of graded index photonic crystals. Appl. Phys. Lett. **93**, 171108 (2008)
8. S. Fan, P.R. Villenueve, J.D. Joannopoulos, E.F. Schubert, Photonic crystal light-emitting diodes. Proc. SPIE **3002**, 67 (1997)
9. D.H. Long, I.-K. Hwang, S.-W. Ryu, J. Korean Phys. Soc. **51**, 1400 (2007)
10. J.J. Wierer, M.R. Krames, J.E. Epler, N.F. Gardner, M.G. Graford, InGaN/GaN quantum-well heterostructure light-emitting diodes employing photonic crystal structures. Appl. Phys. Lett. **84**, 3885 (2004)
11. L.C. Andreani, M. Agio, Photonic bands and gap maps in a photonic crystal slab. IEEE J. Quantum Electron. **38**, 891 (2002)
12. A.L. Bingham, D. Grischkowsky, Terahertz two-dimensional high-Q photonic crystal waveguide cavities. Opt. Lett. **33**, 348 (2008)
13. R. Meisels, O. Glushko, F. Kuchar, Photonics Nanostruct. **10**, 60 (2012)
14. L. Prodan, R. Hagen, P. Gross, R. Arts, R. Beigang, C. Fallnich, A. Schirmacher, L. Kuipers, K.J. Boller, Mid-IR transmission of a large-area 2D silicon photonic crystal slab. J. Phys. D Appl. Phys. **41**, 135105 (2008)
15. M. Skorobogatiy, J. Yang, *Fundamentals of Photonic Crystals Guiding* (Cambridge University Press, Cambridge, 2009)
16. A.F. Oskooi, D. Roundy, M. Ibanescu, P. Bermel, J.D. Joannopoulos, S.G. Johnson, Comput. Phys. Commun. **181**(3), 687 (2010)
17. S.G. Jhonson, J.D. Joannopoulos, Opt. Express **8**, 173 (2001)
18. S.G. Jhonson, P.R. Villenueve, S. Fan, J.D. Joannopoulos, Phys. Rev. B **62**, 8212 (2000)
19. A. Taflove, S.C. Hagness, *Computational Electrodynamics: The Finite-Difference Time-Domain Method* (Artech House, Norwood, MA, 2005)
20. D.M. Sulivan, *Electromagnetic Simulation Using the FDTD Method. Series on RF and Microwave Technology* (IEEE Press, New York, 2000)
21. G.A. Samara, Temperature and pressure dependences of the dielectric constants of semiconductors. Phys. Rev. B **27**, 3494 (1983)
22. S. Adachi, Properties of group-IV,IIIV and IIVI semiconductors. in *Wiley Series in Materials for Electronic and Optoelectronic Applications* (Wiley, England 2005), pp. 195–198
23. M.P. MikhaiIova, in *Handbook Series on Semiconductor Parameters*, vol. 2, ed. by M. Levinshtein, S. Rumyantsev, M. Shur (Singapore, World Scietific, 1999), pp. 180–191
24. R. Sánchez-Cano, N. Porras-Montenegro, Phys. E Low Dimens. Syst. Nanostruct. **43**, 76 (2010)
25. J. Barvestani, S. Dehghan, A.S. Vala, Temperature tunability of cavity-semiconducting waveguide coupling in a two-dimensional photonic crystal. Photon Nanostruct. Fundam. Appl. (2014). doi:10.1016/j.photonics2014.07.002